

UC San Diego

UC San Diego Previously Published Works

Title

Arsenic is a potent co-mutagen of ultraviolet light

Permalink

<https://escholarship.org/uc/item/3xm7z8n5>

Journal

Communications Biology, 6(1)

ISSN

2399-3642

Authors

Speer, Rachel M

Nandi, Shuvro P

Cooper, Karen L

et al.

Publication Date

2023

DOI

10.1038/s42003-023-05659-4

Peer reviewed

## Arsenic is a potent co-mutagen of ultraviolet light

Rachel M. Speer<sup>1,8</sup>, Shuvro P. Nandi <sup>2,3,4,8</sup>, Karen L. Cooper<sup>1</sup>, Xixi Zhou<sup>1</sup>, Hui Yu<sup>5</sup>, Yan Guo<sup>5</sup>, Laurie G. Hudson<sup>1</sup>, Ludmil B. Alexandrov <sup>2,3,4</sup>✉ & Ke Jian Liu <sup>1,6,7</sup>✉

Arsenic enhances the carcinogenicity of ultraviolet radiation (UVR). However, the mechanisms of arsenic-driven oncogenesis are not well understood. Here, we utilize experimental systems to investigate the carcinogenic and mutagenic properties of co-exposure to arsenic and UVR. In vitro and in vivo exposures indicate that, by itself, arsenic is not mutagenic. However, in combination with UVR, arsenic exposure has a synergistic effect leading to an accelerated mouse skin carcinogenesis and to more than 2-fold enrichment of UVR mutational burden. Notably, mutational signature ID13, previously found only in UVR-associated human skin cancers, is observed exclusively in mouse skin tumors and cell lines jointly exposed to arsenic and UVR. This signature was not observed in any model system exposed purely to arsenic or purely to UVR, making ID13, to the best of our knowledge, the first co-exposure signature to be reported using controlled experimental conditions. Analysis of existing skin cancer genomics data reveals that only a subset of cancers harbor ID13 and these exhibit an elevated UVR mutagenesis. Our results report a unique mutational signature caused by a co-exposure to two environmental carcinogens and provide comprehensive evidence that arsenic is a potent co-mutagen and co-carcinogen of UVR.

<sup>1</sup>Department of Pharmaceutical Sciences, College of Pharmacy, University of New Mexico, Albuquerque, NM 87106, USA. <sup>2</sup>Department of Cellular and Molecular Medicine, UC San Diego, La Jolla, CA 92093, USA. <sup>3</sup>Moore's Cancer Center, UC San Diego, La Jolla, CA 92037, USA. <sup>4</sup>Department of Bioengineering, UC San Diego, La Jolla, CA 92093, USA. <sup>5</sup>Sylvester Comprehensive Cancer Center, University of Miami, Miami, FL 33136, USA. <sup>6</sup>Stony Brook Cancer Center, Stony Brook University, Stony Brook, NY 11794, USA. <sup>7</sup>Department of Pathology, Stony Brook University School of Medicine, Stony Brook, NY 11794, USA. <sup>8</sup>These authors contributed equally: Rachel M. Speer, Shuvro P. Nandi. ✉email: [L2alexandrov@health.ucsd.edu](mailto:L2alexandrov@health.ucsd.edu); [kejian.liu@stonybrookmedicine.edu](mailto:kejian.liu@stonybrookmedicine.edu)

Carcinogens are agents that result in cancer formation<sup>1</sup>, with many carcinogens causing cancer by directly generating somatic mutations<sup>2</sup>. Recent experimental studies have also unambiguously described non-mutagenic carcinogens, where cancers were induced in mice by exposing them to suspected human carcinogens without observing an elevation in somatic mutations<sup>3</sup>. Further, prior studies have provided evidence for the existence of co-carcinogens, which are agents that may not be carcinogenic on their own, but they rather promote the effects of other carcinogens<sup>4</sup>. Lastly, limited prior evidence has been offered for co-mutagenic agents, which are generally non-mutagenic but, in combination with another agent, can have synergistic effect leading to a highly accelerated mutagenesis<sup>5</sup>.

Arsenic is a naturally occurring element and a known environmental contaminant found in high concentrations in drinking water within the United States and across the world, particularly from water sourced from wells<sup>6,7</sup>. The International Agency for Research on Cancer has classified arsenic as carcinogenic to humans based on strong evidence linking arsenic exposure to cancers of the lung, bladder, kidney, and skin<sup>8,9</sup>. While skin cancer is commonly associated with exposure to ultraviolet radiation (UVR) from sunlight, arsenic is a known co-carcinogen of UVR<sup>10–12</sup>. Further, epidemiological studies have shown an increased risk for developing UVR-associated skin cancer in populations exposed to high-levels of arsenic and these results have been supported by experimental studies<sup>13–16</sup>. While prior research has shown arsenic inhibits repair of UVR-induced DNA damage<sup>17–19</sup> the mutagenic properties of arsenic co-exposure have not been well understood.

Analysis of mutational signatures allows elucidating the mutagenic processes that lead to cancer<sup>20</sup>. Previously, we and others have described more than 100 different mutational signatures including ones associated with environmental carcinogens, failure of DNA-repair pathways, infidelity of replicating polymerases, chemotherapeutics, and many others<sup>21,22</sup>. Only one study has investigated the mutational patterns of arsenic in human cancer by inconclusively examining a single never-smoker lung cancer patient chronically exposed to arsenic<sup>23</sup>. Further, while induced pluripotent stem cell lines have been exposed to arsenic, no arsenic mutational signature was found<sup>24</sup>. In contrast, exposure to UVR from sunlight is known to induce specific DNA damage and several distinct UVR-associated mutational signatures have been identified in human tumors, normal human tissues, and experimental systems<sup>25–29</sup>.

Notably, mutational signatures of single base substitutions (SBSs), termed COSMIC signatures SBS7a/b/c/d, have been found at extremely high levels in most cancers of the skin<sup>22</sup> as well as in experimental systems exposed to UVR<sup>24</sup>. SBS7a/b are characterized by C > T mutations at dipyrimidines and have been associated with DNA damage due to UVR, including both 6,4-photoproducts and cyclobutane pyrimidine dimers (CPDs)<sup>30–32</sup>. Signatures SBS7c and SBS7d are characterized by T > A and T > C mutations, respectively, and while these UVR signatures are exclusively found in cancers of the skin, their etiology remains mysterious<sup>22,32,33</sup>.

A doublet-base substitution (DBS) signature, termed DBS1, has also been found at high levels in human skin tumors, normal human skin tissues, and experimental systems exposed to UVR<sup>25–29</sup>. Signature DBS1 exhibits almost exclusively CC > TT mutations and it has been attributed to mis-replication of CPDs<sup>22</sup>. Additionally, a mutational signature of small insertions and deletions (indels), termed, COSMIC signature ID13, has been found exclusively in cancers of the skin in sun exposed areas and, thus, it has been attributed to exposure to ultraviolet light<sup>22,33</sup>. ID13 exhibits a particular pattern that includes a deletion of a single thymine at a thymine-thymine dimer<sup>33</sup>.

In this study, we leverage well controlled in vitro and in vivo co-exposures in combination with whole-genome sequencing and mutational signatures analysis to investigate the carcinogenic and mutagenic properties of arsenic and solar-simulated UVR co-exposure. Our experimental findings reveal that, in combination with UVR, arsenic exposure has a synergistic effect leading to an enhanced mouse skin carcinogenesis as well as to more than 2-fold enrichment of UVR mutational burden. Importantly, signature ID13 is uniquely due to arsenic and UVR co-exposure and, comparisons with genomics data from previously generated skin cancers demonstrate that ID13 is found exclusively in a large proportion of human skin cancers with an elevated UVR mutagenesis. Our results demonstrate that arsenic is a potent co-mutagen of ultraviolet light that amplifies UVR mutagenesis and that generates a unique mutational signature commonly found in human cancers of the skin.

## Results

**In vitro and in vivo experimental designs.** To examine the mutagenic properties of co-exposures to arsenic (As) and UVR, we used both in vitro and in vivo models. Specifically, an immortalized keratinocyte cell line, N/TERT1<sup>34</sup>, was utilized under the following conditions: (i) no treatment (NT); (ii) irradiation with 3 kJ/m<sup>2</sup> solar simulated UVR, i.e., a UVA (320–400 nm) and UVB (280–320 nm) spectrum with an emission ratio of 13:1 for UVA:UVB; (iii) treatment with arsenic (1 μM); and (iv) pre-treatment with arsenic (1 μM) for 24 hours followed by irradiation with UVR (3 kJ/m<sup>2</sup>). Arsenic exposures were continued for 24 hours (for a total arsenic exposure of 48 h) post-UVR irradiation during the time in which UVR generated DNA damage is likely being repaired. All cells were cultured for an additional 24 hours after their respective exposures and, subsequently, subjected to barrier bypass-clonal expansions<sup>35</sup> and whole-genome sequencing (Fig. 1a). The selected arsenic and UVR exposure levels align with previous studies investigating arsenic-UVR co-carcinogenesis<sup>36–38</sup>. In most cases, the combined exposure of arsenic and UVR resulted in similar levels of cytotoxicity to the ones due to UVR exposure alone (Fig. 1b); cytotoxicity was measured relative to the NT group. Consistent with conditions used in previous evaluation of environmental carcinogens<sup>24</sup>, we clonally expanded cells from exposures resulting in approximately 50% relative cell death (Fig. 1b).

To confirm the observed in vitro results, we also utilized a SKH-1 hairless mouse model<sup>39</sup> where mice were separated into four groups ( $n = 14$  for each group), including: (i) a NT group; (ii) a group where mice were exposed to arsenic in their drinking water (5 mg/l); (iii) a group where mice were exposed to UVR three times per week (14 kJ/m<sup>2</sup> solar simulated UVR); and (iv) a group where mice were exposed to arsenic in their drinking water (5 mg/l) and exposed to UVR three times per week (14 kJ/m<sup>2</sup>; Fig. 1c). The total arsenic exposure for arsenic treated groups was approximately 37 weeks. The level of 5 mg/l arsenic used in this study is higher than the 0.01 mg/l maximum contaminant level set by the U.S. EPA<sup>40</sup>. However, it is estimated 2.1 million people are exposed to arsenic exceeding the MCL through unregulated domestic well water in the United States reporting up to 2.9 mg/l levels<sup>41</sup>. In addition, mice are faster metabolizers of arsenic compared to humans, and thus, higher arsenic concentrations are required to induce responses similar to those that would be seen in humans at lower concentrations<sup>42,43</sup>. No overt toxicity was observed in mice exposed to 5 mg/l arsenic. The UVR exposure chosen is approximately half the minimal exposure level that results in erythema (reddening of the skin) and is therefore relevant to environmental exposures. No tumors developed in mice in the NT or arsenic alone groups, however, tumors

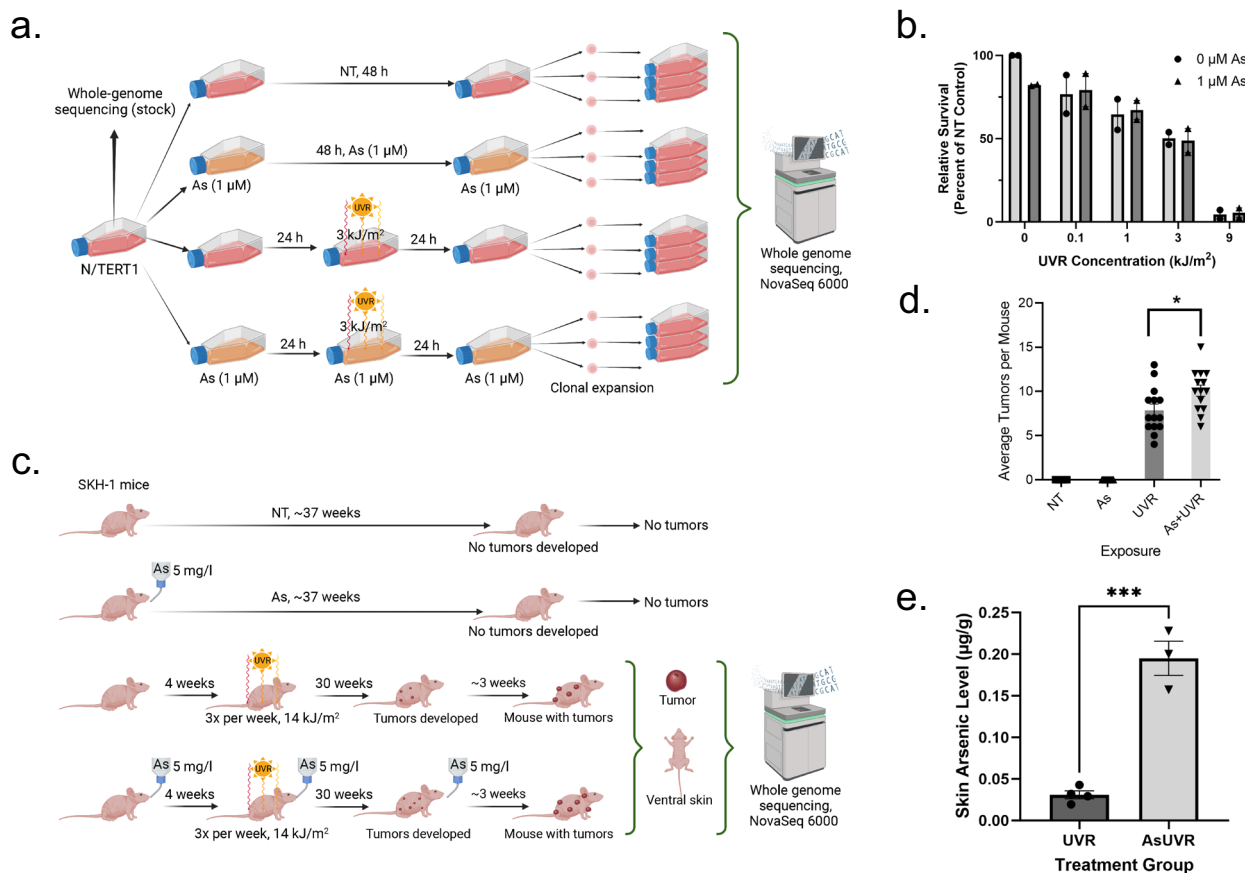


**Fig. 1 Experimental design for mutational signatures co-exposure analysis.** **a** Experimental design for N/TERT1 cells, where somatic mutations were called from clones expanded from treatment groups, no treatment (NT) control, arsenic (As), ultraviolet light radiation (UVR), and As plus UVR, against the bulk sequenced stock. **b** Y-axis reflects the relative survival of exposed cells measured using the percentage of clonogenic survival compared to survival of the NT control. The x-axis corresponds to the total amount of energy delivered per unit area. The circles reflect individual values for cell line experiments without arsenic pre-treatment, while the triangles correspond to individual values for cell line experiments pre-treated with arsenic (1 μM). Average values are displayed as light gray bars for cells without arsenic pre-treatment and dark gray bars for cells pre-treated with arsenic. No statistically significant difference in survival were observed in cells pre-treated with arsenic and cells without arsenic pre-treatment (two-sided *t*-test; *n* = 2 derived from 2 independent experiments with 4 technical replicates each for all experimental conditions). The experimental conditions used in this study utilized exposure levels leading to 50% relative survival in N/TERT1 cells in alignment with previously published studies<sup>24</sup>. **c** Experimental design utilizing SKH-1 hairless mouse model, where mice were separated into four groups, including: a NT group; arsenic exposed group; UVR exposed group; and As plus UVR exposed group. No tumors developed in NT or arsenic alone groups. Somatic mutations in skin tumors from UVR as well as As plus UVR exposed mice were identified by comparing the sequenced tumor tissues to the sequenced ventral (non-UVR exposed) normal skin from the same animal. **d** Y-axis reflects the average number of tumors per mouse, while the x-axis corresponds to the different experimental conditions. The tumorigenicity for the mouse model shows arsenic significantly enhances tumor burden in UVR exposed mice (*p*-value < 0.05; two-sided *t*-test; *n* = 14 for all conditions). **e** Y-axis represents the arsenic level in skin from mice included in the study, while the x-axis corresponds to the study group. Arsenic skin levels were significantly higher in the arsenic exposed mice compared to those not exposed (*p*-value < 0.001; two-sided *t*-test; *n* = 4 for the UVR group and *n* = 3 for the AsUVR group). Data represent the mean ± SEM. Statistical details are reported in the Methods section. Panels **a** and **c** were created with BioRender.com.

developed in the UVR group and tumor burden was 1.3-fold enhanced by co-exposure with arsenic (*p*-value: 0.0265; two-sided *t*-test; Fig. 1d). A significant increase in arsenic in the skin of animals from which tumors were sequenced for this study was observed (*p*-value: 0.0003; two-sided *t*-test; Fig. 1e). The mean level of arsenic in arsenic-exposed mouse skin was 0.19 μg/g, which is lower than levels measured in hair (2.29 μg/g) and nails (4.73 μg/g) from humans exposed to arsenic and within the range reported in hair (0.01–0.61 μg/g) and skin (0.06–3.3 μg/g) from populations with mixed arsenic exposures<sup>44</sup>.

**Arsenic affects UVR mutagenesis in vitro.** Somatic mutations were identified from all whole-genome sequenced N/TERT1 cells by bioinformatically comparing them to the whole-genome sequenced stock cells (Methods; Fig. 1a). Statistical comparisons

for the N/TERT1’s mutational landscapes were performed amongst controls and the three different types of exposures using one-way ANOVA with Tukey post hoc correction for multiple comparisons (Fig. 2a, c). Arsenic alone did not increase the total numbers of SBSs, DBSs, or indels in N/TERT1 cells when compared to the ones found in NT controls (Fig. 2a). In contrast, UVR exposure resulted in a significant increase of 3.9-fold for SBSs and 10-fold for DBSs when compared to NT controls (*p*-values: 0.0040 and 0.0345, respectively). C > T, T > C, C > A, T > A, and T > G substitutions were significantly elevated when compared to their levels in untreated controls (*p*-values: 0.0074, 0.0476, 0.0152, 0.0459, and 0.0309, respectively; Supplementary Fig. 1a–d). Importantly, samples co-exposed to arsenic and UVR exhibited approximately 1.8- and 2.1-fold significant enrichment of SBSs and DBSs, respectively, when compared to samples

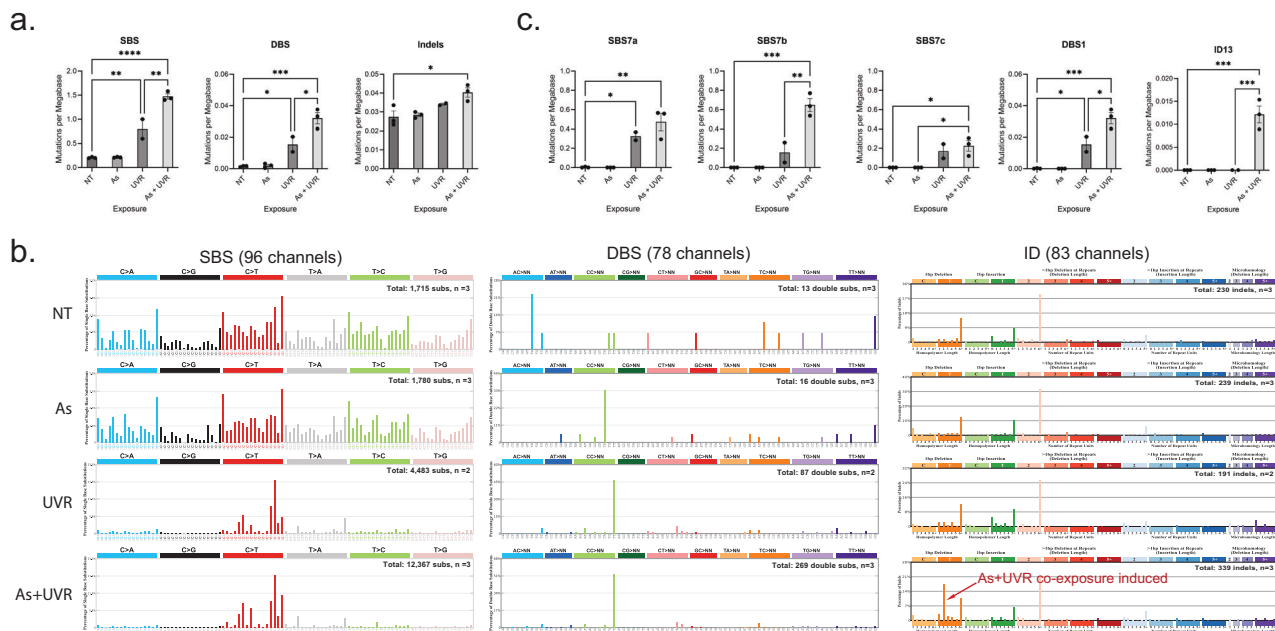


**Fig. 2** Arsenic enhances somatic mutations imprinted by ultraviolet light in N/TERT1 cells. **a** Y-axes reflect the amounts of substitutions (SBS; left), doublets (DBS; middle), or small insertions and deletions (Indels; right) measured in somatic mutations per megabase. X-axes correspond to the different types of exposures including: no treatment (NT) control, arsenic (As), ultraviolet light radiation (UVR), and As plus UVR. Bar plots represent the mean  $\pm$  SEM; individual biological replicates are shown as black circles. **b** Patterns of single base substitutions (SBS) are shown on the left using the SBS-96 classification scheme<sup>65</sup> on the x-axes. Patterns of doublet base substitutions (DBS) are shown in the middle using the DBS-78 classification scheme<sup>65</sup> on the x-axes. Patterns of small insertions and deletions (ID) are shown on the right using the ID-83 classification scheme<sup>65</sup> on the x-axes. Each plot represents the average mutational profile of each treatment group across all samples in that group. Y-axes are scaled differently in each plot to optimally show each average mutational pattern with the y-axes reflecting the percentage of mutations for the respective mutational scheme. **c** Y-axes reflect the amounts of COSMIC mutational signatures measured in somatic mutations per megabase. X-axes correspond to the different types of exposures. Bar plots represent the mean  $\pm$  SEM; individual biological replicates are shown as black circles. Significance was evaluated using one-way ANOVA with Tukey's multiple comparisons test;  $n = 3$  for NT, As, and As plus UVR and  $n = 2$  for UVR alone derived from independent clones. \* $p$ -value  $< 0.05$ , \*\* $p$ -value  $< 0.01$ , \*\*\* $p$ -value  $< 0.005$ , \*\*\*\* $p$ -value  $< 0.001$ . Statistical details are reported in the Methods section.

exposed to UVR alone ( $p$ -values  $< 0.05$ ). Specifically, C  $>$  T mutations contributed most mutations in UVR exposed cells and arsenic co-exposure resulted in 2.2-fold increase of these mutations compared to UVR alone ( $p$ -value: 0.001; Supplementary Fig. 1a). Arsenic also significantly increased C  $>$  G mutations compared to UVR alone ( $p$ -value: 0.0112). The total number of indels was 1.5-fold elevated in samples co-exposed to arsenic and UVR when compared to NT control ( $p$ -value: 0.0177) but not compared to UVR alone (Fig. 2a).

The mutational patterns of arsenic exposed cells were identical to the ones of non-treated controls for both substitutions and indels (cosine similarity: 0.97; Fig. 2b). The numbers of doublets were too few to perform a comparison between NT controls and arsenic exposed cells. In contrast, UVR-exposed N/TERT1 cells exhibited a distinct pattern of C  $>$  T substitutions at dipyrimidines as well as high levels of CC  $>$  TT doublets (Fig. 2b). Further, the mutational patterns of both substitutions and doublets were remarkably similar between cells exposed only to UVR and cells exposed jointly to arsenic and UVR (cosine similarity: 0.97). Nevertheless, the pattern of small insertions and deletions was different between these two exposures with a striking elevation of single thymine deletions at a thymine-thymine dimers in the cells exposed to arsenic plus UVR (Fig. 2b). Additionally, an examination of previously generated datasets<sup>24</sup> revealed that the substitution patterns of UVR in N/TERT1 cells are similar to the ones observed in human induced pluripotent stem cells (iPSCs) exposed to UVR (cosine similarity: 0.96). In contrast, a distinct difference can be seen in the iPSC indel profile which lacks the thymine deletion at thymine-thymine dimers observed in arsenic

and UVR co-exposed N/TERT1 cells (cosine similarity: 0.35). Overall, the indel profile of UVR-exposed iPSC cells was consistent with the one of UVR-exposed N/TERT1 cells and neither UVR-exposed iPSC cells nor UVR-exposed N/TERT1 cells harbored the unique indel pattern observed in N/TERT1 cells co-exposed to arsenic and UVR.

Analysis of COSMIC mutational signatures revealed that three of the four UVR-associated SBS signatures, SBS7a/b/c, as well as the UVR-associated signatures DBS1 and ID13 were found in N/TERT1 cells exposed to UVR (Fig. 2c). No UVR-associated signatures were identified in untreated N/TERT1 cells or in N/TERT1 exposed purely to arsenic. Co-exposure to arsenic resulted in a 4.2-fold increase of SBS7b and 2.1-fold increase of DBS1 ( $p$ -value: 0.0015 and 0.0143, respectively) but not to a statistically significant elevation of signatures SBS7a or SBS7c compared to UVR alone. Remarkably, signature ID13 was exclusively identified in the N/TERT1 cells co-exposed to arsenic and UVR but not in cells exposed purely to UVR ( $p$ -value: 0.0005; Fig. 2c). Consistent with the analysis of COSMIC mutational signatures, analysis of de novo signatures revealed an elevation of SBS signatures as well as an indel signature, resembling ID13, found exclusively in samples co-exposed to UVR and arsenic (Supplementary Fig. 2).

**Arsenic affects UVR mutagenesis in vivo.** The performed in vitro exposures were complemented by almost identical exposures in a SKH-1 hairless mouse model (Fig. 1c). No tumors were observed in the NT group ( $n = 14$ ) or in mice exposed to arsenic alone ( $n = 14$ ; Fig. 1d). For a subset of UVR-exposed



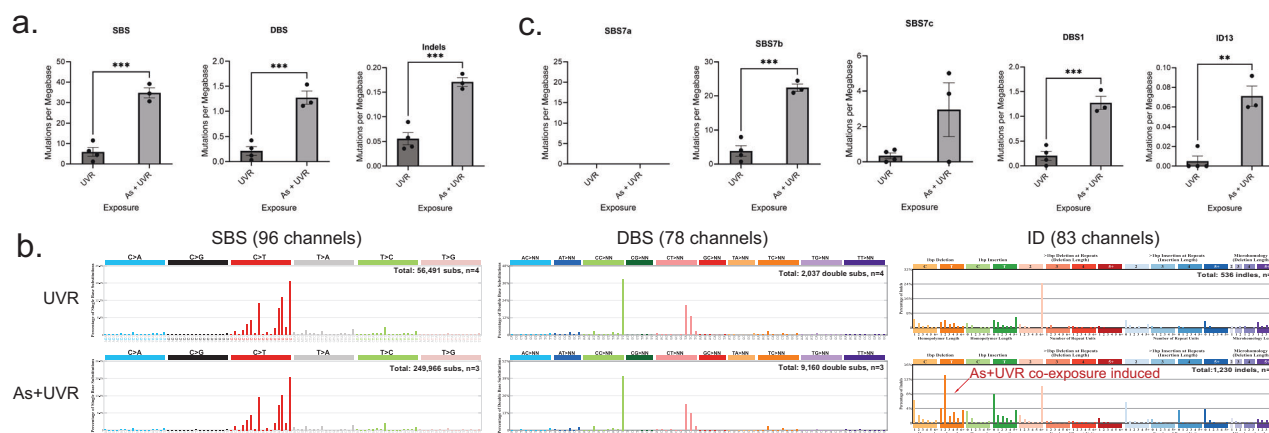


**Fig. 3** Arsenic enhances somatic mutations imprinted by ultraviolet light in skin cancers from SKH-1 hairless mice. **a** Y-axes reflect the amounts of substitutions (SBS; left), doublets (DBS; middle), or small insertions and deletions (Indels; right) measured in somatic mutations per megabase. X-axes correspond to the different types of exposures including: ultraviolet light radiation (UVR), and arsenic (As) plus UVR. Bar plots represent the mean  $\pm$  SEM; individual biological replicates are shown as black circles. **b** Patterns of single base substitutions (SBS) are shown on the left using the SBS-96 classification scheme<sup>65</sup> on the x-axes. Patterns of doublet base substitutions (DBS) are shown in the middle using the DBS-78 classification scheme<sup>65</sup> on the x-axes. Patterns of small insertions and deletions (ID) are shown on the right using the ID-83 classification scheme<sup>65</sup> on the x-axes. Each plot represents the average mutational profile of each treatment group across all samples in that group. Y-axes are scaled differently in each plot to optimally show each average mutational pattern with the y-axes reflecting the percentage of mutations for the respective mutational scheme. **c** Y-axes reflect the amounts of COSMIC mutational signatures measured in somatic mutations per megabase. X-axes correspond to the different types of exposures. Bar plots represent the mean  $\pm$  SEM; individual biological replicates are shown as black circles. Significance was evaluated using FDR corrected two-sided *t*-tests;  $n = 4$  for UVR alone and  $n = 3$  for As plus UVR derived from individual animals. \*\**q*-value < 0.01, \*\*\**q*-value < 0.005. Bar plots represent the mean  $\pm$  SEM; individual replicate values are shown as black circles. Statistical details are reported in the Methods section.

mice, a tumor and matched normal skin tissue from the ventral (non-UVR exposed) side of each animal were whole-genome sequenced and, subsequently, bioinformatically compared to derive somatic mutations in the tumor tissue (Methods; Fig. 1c). Statistical comparisons between the mutational landscapes of the tumors in mice exposed to UVR alone and the tumors in mice co-exposed to arsenic and UVR were performed using FDR-corrected two-sided *t*-tests (Methods).

Tumors from mice co-exposed to arsenic and UVR exhibited approximately 6-fold enrichment of substitutions, 6-fold enrichment of doublets, and 3-fold enrichment of indels when compared to tumors from mice only exposed to UVR (*q*-values: 0.0009, 0.0009, 0.0009, respectively; Fig. 3a). Similar to N/TERT1 cells, all types of single base substitutions and doublet base substitutions were significantly elevated in tumors due to co-exposure to arsenic and UVR (*q*-values < 0.05; Supplementary Fig. 1e–h). Further, both insertions and deletions were found to be increased approximately 3-fold in tumors from co-exposed mice when compared to tumors due to UVR alone (*q*-values: 0.0014 and 0.0023, respectively; Supplementary Fig. 1g, h).

A distinct pattern of C > T substitutions at dipyrimidines was observed in all mouse tumors (Fig. 3b). The pattern was identical between tumors due to UVR alone and tumors due to arsenic and UVR (cosine similarity: 0.99; Fig. 3b). Interestingly, this pattern of single base substitutions is also similar to previous data from mouse cell lines<sup>27</sup> exposed to UVR (cosine similarity: 0.98) while differing from the substitution patterns observed in N/TERT1 cells (cosine similarity: 0.84) or in UVR-associated human skin cancers (cosine similarity: 0.80)<sup>25</sup>. Specifically, UVR-imprinted patterns in mouse tumors and mouse cell lines have a distinctly high peak of C > T mutations at TpTpT trinucleotides (mutated base underlined; Fig. 3b) which is absent in human tumors<sup>27</sup> or in human cell lines (Fig. 2b). Similarly, CC > TT and CT > NN dinucleotides were observed in all UVR-associated mouse tumors (Fig. 3b). The CC > TT mutational pattern in mouse tumors was similar to the one observed in N/TERT1 cells (Fig. 2b) but the

CT > NN dinucleotides were unique for mouse tumors and mouse cell lines<sup>27</sup> and CT > NN dinucleotides have not been found in human skin cancers or in UVR-exposed human cell lines. Importantly, similar to human cell lines, the mouse tumors exhibited a striking elevation of single thymine deletions at thymine-thymine dimers in the cells co-exposed to UVR and arsenic (Fig. 3b).

Evaluating the COSMIC mutational signature in the UVR-exposed mouse tumors elucidated the presence of signatures SBS7b, SBS7c, DBS1, and ID13. Consistent with the in vitro observations, signatures SBS7b and DBS1 were almost 6-fold enriched in the tumors due to co-exposure to arsenic and UVR (*q*-values: 0.0006 and 0.001, respectively; Fig. 3c). Further, as in the cell line experiments, signature ID13 was exclusively identified in tumors due to co-exposure to UVR and arsenic but not in tumors purely due to UVR exposure (Fig. 3c). Consistent with the analysis of COSMIC mutational signatures and the observations in N/TERT1 cell lines, analysis of de novo signatures from mouse tumors revealed an elevation of SBS signatures and an indel signature, resembling ID13, highly elevated in samples co-exposed to UVR and arsenic (Supplementary Fig. 2).

#### Evaluating arsenic-like co-exposures in human skin cancer.

Our experimental results revealed that ID13 is generated exclusively in samples jointly co-exposed to arsenic and UVR (Figs. 2 and 3). To the best of our knowledge, this study is the first to report ID13 in any experimental system likely due to prior studies focusing purely on UVR exposure without any additional co-exposures<sup>27</sup>. Importantly, ID13 was not observed in any sample exposed purely to UVR (Figs. 2 and 3), indicating that a co-exposure to arsenic or to another co-mutagen with similar properties is required for generating signature ID13.

Next, we interrogated 302 previously published<sup>45</sup> whole-exome sequenced basal cell carcinomas (BCCs) and utilized signature ID13 as a biomarker of potential co-exposure to UVR and arsenic (or another arsenic-like agent). Specifically, whole-exome

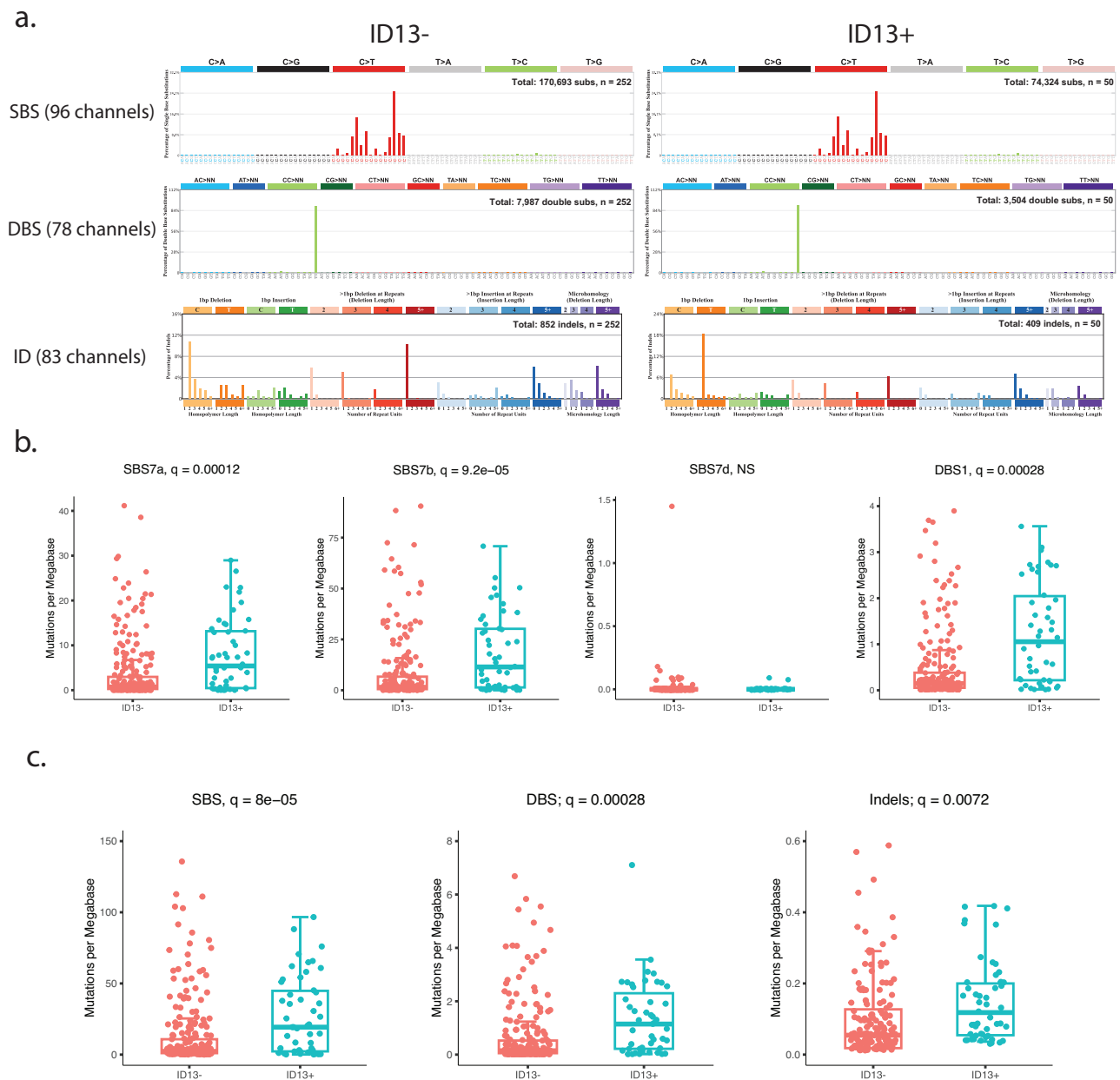


**Fig. 4 An evaluation of UVR and arsenic-like co-exposure in human basal cell carcinomas.** **a** Patterns of single base substitutions (SBS) in basal cell carcinomas (BCCs) are shown on the left using the SBS-96 classification scheme<sup>65</sup> on the x-axes. Patterns of doublet base substitutions (DBS) in BCCs are shown in the middle using the DBS-78 classification scheme<sup>65</sup> on the x-axes. Patterns of small insertions and deletions (ID) in BCCs are shown on the right using the ID-83 classification scheme<sup>65</sup> on the x-axes. Each plot represents the total mutational profile of ID13 negative and ID13 positive BCCs groups across all samples in that group. Y-axes are scaled differently in each plot to optimally show each average mutational pattern with the y-axes reflecting the percentage of mutations for the respective mutational scheme. Total refers to the number of somatic mutations, while n refers to the number of samples. **b** Mutations per megabase attributed to COSMIC mutational signatures operative in basal cell carcinomas. Each dot reflects the mutations per megabase attributed to each COSMIC signature in each sample. **c** Overall number of substitutions (SBS; left), doublets (DBS; middle), or small insertions and deletions (indels; right) measured in somatic mutations per megabase from BCC patients. X-axes correspond to the group including absent of ID13 (ID13-) and presence of ID13 (ID13+). The bounds of the boxplots represent the interquartile range divided by the median, and Tukey-style whiskers extend to a maximum of  $1.5 \times$  interquartile range beyond the box. Statistically significant results from FDR corrected two-sided *t*-tests are denoted as *q*-values. In both panels, basal cell carcinomas were separated on samples containing ID13 ( $n = 50$ ) and basal cell carcinomas without any ID13 ( $n = 252$ ).

sequenced BCCs with both  $\geq 5\%$  of all mutations and  $\geq 2$  mutations attributed to ID13 were classified as containing the signature. Based on these criteria 16.5% of BCC samples exhibited ID13 and the SBS, DBS, and indel mutational profiles of BCCs were partitioned into ID13 negative and ID13 positive samples

(Fig. 4a). The SBS and DBS patterns were identical between ID13 negative and ID13 positive BCC sample (cosine similarities  $>0.98$ ; Fig. 4a). Statistically significant elevations of signatures SBS7a, SBS7b, and DBS1 ( $q$ -values  $<0.05$ ; Fig. 4b) were found within BCCs samples containing ID13 when compared to samples

without ID13. Furthermore, consistent with our experimental results that samples co-exposed to arsenic and UVR exhibited a much higher burden of single and doublet substitutions (Figs. 2a and 3a), the BCC samples harboring ID13 exhibited more than 2.1-fold elevation of both single base substitutions and doublet base substitutions ( $q$ -values < 0.05; Fig. 4c). Additionally, 107 whole-genome sequenced melanomas<sup>46</sup> were also examined with samples classified as harboring ID13 when both  $\geq 5\%$  of all mutations and  $\geq 100$  mutations were attributed to ID13. The evaluation yielded similar results with 42% of melanoma genomes harboring ID13 and exhibiting a highly elevated mutational burden of single and doublet substitutions (Supplementary Fig. 4).

## Discussion

In this study, we applied mutational signatures analysis to whole-genome sequencing data from well-controlled in vitro and in vivo experimental systems to elucidate the carcinogenic and mutagenic potentials of arsenic and ultraviolet light. As expected, the mutational patterns found on the genomes of UVR-exposed cell lines and on mouse cancers were consistent with the set of known UVR mutational signatures derived from human skin cancers. Exposing cell lines purely to an environmentally relevant concentration of arsenic neither caused an elevated mutational burden nor a specific mutational signature. Further, mice exposed only to arsenic did not develop any tumors. Nevertheless, the co-exposure to arsenic and UVR resulted in enhanced carcinogenesis and a synergistic elevation of UVR mutagenesis. It was notable that C > T mutations, which are known to result from unrepaired CPD lesions<sup>47</sup>, were particularly enhanced by arsenic exposure. This result is in alignment with previous work showing arsenic inhibits nucleotide excision repair (NER), the predominant pathway responsible for repair of CPD lesions<sup>15,18,19,48</sup>. Further, we have previously shown arsenic can displace zinc from zinc finger proteins, specifically those involved in NER such as XPA<sup>15,49–51</sup>. Therefore, it is likely arsenic inhibits NER through disruption of zinc finger protein function. Our future work will further confirm these effects by evaluating protein-protein interactions and function.

Importantly, a specific mutational signature, ID13, was found exclusively in samples co-exposed to arsenic and UVR. ID13 is characterized predominantly by the deletion of T in a TT homopolymer context<sup>52</sup>. The accumulation of these mutations may be due to the persistence of UVR-induced DNA damage at pyrimidine dimers, which are well-documented<sup>53,54</sup> and subsequent inhibition of damage repair by arsenic and potentially slippage during subsequent replication over damage converting this damage to mutations. To the best of our knowledge, this is the first report of a unique mutational signature caused by a co-exposure to two environmental carcinogens and the first comprehensive evidence that arsenic is a potent co-mutagen of UVR.

Our examination of human skin cancers revealed that 16.5% of basal cell carcinomas and 42% of human melanomas harbor signature ID13 in their genomes. This is a striking result as, based on our experimental data and previous experimental interrogations<sup>24,27</sup>, exposure to UVR alone cannot induce signature ID13. Further, consistent with these experimental findings, human skin cancers with ID13 exhibited an elevated burden of single and doublet substitutions, thus, further implicating an additional co-exposure. Supporting this hypothesis, it is estimated that 2.1 million people are exposed to arsenic levels above the 10 ppb maximum contaminant level set by the U.S. Environmental Protection Agency<sup>41</sup>. These exposures put a significant proportion of the U.S. population at risk

of arsenic and UVR co-exposure, however, arsenic exposure data from patients would be required to directly correlate ID13 with arsenic-UVR co-exposure. Moreover, separating previously generated cancer genomes based on the presence of ID13 is limited by the resolution of bioinformatics tools which generally do not allow detecting mutational signatures that account for less than 5% of all mutations within a single sample<sup>55</sup>. Nevertheless, our results suggest that likely a large proportion of human skin cancers are formed due to co-exposure of UVR and arsenic or due to co-exposure of UVR and another co-carcinogenic agent with similar co-mutagenic properties to the ones of arsenic.

## Methods

**Cell culture.** An hTERT immortalized non-cancerous human keratinocyte cell line (N/TERT1), established from a male neonate in a previous study<sup>34</sup> was used in this study. N/TERT1 cells respond similarly as primary keratinocytes under experimental conditions<sup>56</sup>. N/TERT1 cells were cultured as monolayers with serum-free DermaLife K Keratinocyte Medium (Lifeline Cell Tech) supplemented with DermaLife K Life-Factors in a humidified incubator at 37°C and 5% CO<sub>2</sub>. Cells were sub-cultured with 0.05/0.02% Trypsin/EDTA (Lifeline Cell Tech) every 3–5 days. Although N/TERT1 is a clonally derived cell line, these cells were established >20 years ago. Through normal passaging, single nucleotide variants arise creating a heterogeneous population. Therefore, to reduce noise in the mutational signatures data N/TERT1 were subcloned and a single clone (the grandparent clone) was selected for seeding all experiments. Cells were routinely tested to be negative for mycoplasma and screened for chromosome stability.

**Ultraviolet radiation (UVR) exposure.** Solar simulated UVR (UVR) exposures were performed using an Oriel 1600 Watt Solar Ultraviolet Simulator (Oriel Corp., Stratford, CT). This solar simulator produces a high intensity UVR beam in both the UVA (320–400 nm) and UVB (280–320 nm) spectrum with an emission ratio of 13:1 (UVA:UVB). The proportion and intensity of UVA/UVB was measured using an ILT2400 radiometer equipped with UVA (SED033), UVB (SED240) and UVC (SED270) detectors (International Light Technologies; Peabody, MA). In vivo exposures were at 14 kJ/m<sup>2</sup> providing approximately 0.5 minimum erythema dose (MED). Measurements were made with Erythema UV and UVA intensity meter (Solar Light Co., Inc., Philadelphia, PA) to estimate MED. Animal UVR dosing was conducted in groups of 4–6 with animals allowed to move freely within the exposure enclosure. Cells and animals were kept in the dark during transport to and from the UVR exposure lamp.

**Cell exposures.** Arsenic stock solutions of inorganic arsenic as sodium meta-arsenite (purity >99%; Fluka Chemie) were prepared in double distilled water and filtered through a 0.2  $\mu$ m filter. For all experiments cells were seeded and allowed to rest for 48 hours before treatment. Cells were pre-treated with 1  $\mu$ M arsenic for 24 hours before exposure to 3 kJ/m<sup>2</sup> solar simulated ultraviolet light (ssUVR). Arsenic exposure was continued for 24 hours post ssUVR exposure and clones were expanded for DNA extraction and sequencing. DNA from each clone was extracted using the QIAamp® DNA Mini Kit (Qiagen).

**Cytotoxicity assay.** Cytotoxicity was determined using a clonogenic survival assay<sup>57</sup>. N/TERT1 cells were seeded and allowed to grow for 48 hours before treatment with 0 or 1  $\mu$ M arsenic. After 24 hours, cells were exposed to increasing UVR doses. Cells were



harvested immediately after UVR exposure and re-seeded in 100 mm dishes at colony forming density (300 cells/dish). After colony formation cells were fixed, stained with crystal violet, and colonies were counted. Four dishes per treatment group were included and results are expressed as relative survival, which was derived from the number of colonies per treatment group divided by the number of colonies in the control multiplied by 100.

**In vivo exposures and tissue collection.** Male SKH-1 mice (21–25 days old) were purchased from Charles River Laboratories (Wilmington, MA). These studies were performed under an approved Institutional Animal Care and Use Committee (IACUC) protocol (#22-201244-HSC). Animals were housed by treatment group and administered arsenite (5 mg/l) in the drinking water for the duration of the study. Water was freshly prepared and changed every second day, and consumption monitored. There was equivalent water consumption between control and arsenic treated groups, and all animals were provided standard mouse chow ad lib. After 28 days of arsenic treatment, animals were exposed to UVR (14 kJ/m<sup>2</sup>; ~0.5 minimal erythema dose [MED]) 3 times per week until the development of tumors (30 weeks). There were unavoidable UVR lamp issues during weeks 8 and 9 where animals were not UVR exposed. Water treatment continued for an additional 4 weeks to allow for tumor growth prior to collection. Tumor number by animal was determined once per week by physical palpation and counted if at least 1 mm in diameter. Some tumors regressed over time and only tumors that persisted for at least 3 weeks were included in the total count. Animals were euthanized using CO<sub>2</sub> followed by cervical dislocation and tissues collected. Tissues collected included kidney, liver, spleen, ventral skin (UVR naïve), dorsal skin (UVR exposed) and skin tumors. Tissues were collected in 10% neutral buffered formalin, RNAlater, snap-frozen, and epidermal scrapings obtained from both ventral and dorsal skin. We have complied with all relevant ethical regulations for animal use.

**Metals analysis of mouse skin.** Snap-frozen or RNAlater preserved and frozen mouse skin tissues were thawed on ice then a portion of the tissue was weighed and placed in a metal-free tube. Samples from RNAlater were blotted dry before weighing. All samples were allowed to dry fully before being weighed again and digested. Tissues were digested in 0.5 ml of 70% trace-element free HNO<sub>3</sub> at 90 °C for 4 h. Tubes were visually inspected, and digestion continued if samples were not fully digested. Samples were diluted to a final volume of 10 ml with milliQ water then a 1 ml aliquot taken and further diluted with milliQ water to 3 ml giving a final acid concentration of 1.75%. Samples were transferred to the Integrated Molecular Analysis Core at the University of New Mexico Center for Metals in Biology & Medicine for inductively coupled plasma mass spectrometry (ICP-MS) analysis. For quality control purposes, a clean tube with no tissue was carried through the digestion procedure and analyzed with each group of samples. Blanks and calibration standards were run at the beginning and end of the analysis. Internal reference standards were included in all analyses to account for matrix effects.

**DNA extraction from skin tumors and UVR naïve skin.** Snap-frozen skin tumors (1.5–2 mm in diameter) and UV naïve skin sections (0.5–1 cm<sup>2</sup>) were thawed on ice then removed from the vial and placed on a glass plate previously cleaned with 70% ethanol and RNAzap (Thermo Fisher Scientific). Tissue was minced into small pieces with a pair of clean scalpels and transferred to clean RNase/DNase free tubes. Clean blades were used, and the mincing surface sanitized between samples to limit

cross-contamination. Genomic DNA was extracted using the DNeasy Blood and Tissue kit (Qiagen) following the manufacturers recommendations. For the initial digestion step, 180 µl ATL buffer and 20 µl Proteinase K was added to each sample, vortexed thoroughly, then incubated at 50 °C for 2 hours with vortexing every 15 min. The remaining steps followed the kit's directions exactly. DNA was eluted from the column with 2 consecutive additions of 50 µl of the AE buffer supplied with the kit. DNA concentration and quality was determined using Qubit (Thermo Fisher Scientific). Samples were subsequently diluted to the required concentrations for whole-genome sequencing.

**Whole-genome sequencing.** DNA from in vitro and in vivo experiments was sent to Novogene (Sacramento, CA) and library preparation was performed using the NEBNext® DNA Library Prep Kit (New England Biolabs) following the manufacturer's recommendations. Qualified libraries were sequenced on an Illumina platform to 30x coverage according to effective concentration and data volume.

**Identification of somatic mutations from whole genome bulk sequencing.** Raw sequence data were downloaded to the Triton Shared Compute Cluster (TSCC) from ftp server link shared by Novogene (Sacramento, CA). All the post-sequencing analysis was performed within TSCC at UC San Diego. A schematic of the somatic mutations calling process is described in Supplementary Fig. 5. This methodology for identification of somatic mutations from bulk sequencing data follows established approaches from large genomics consortia<sup>46</sup>. Briefly, quality assurance of the raw FASTQ files were evaluated using FastQC (Version 0.12.0) and Mosdepth (Version 0.3.4)<sup>58,59</sup>. Raw sequence reads were aligned to the human reference genome GRCh38 for N/TERT1 data and GRCm39 for mouse data. The aligned reads were marked duplicated using MarkDuplicates (Picard) from GATK (Version 4.0.11.0)<sup>60</sup>. For human cell lines, concordance between exposed and stock samples were evaluated using Conpair<sup>61</sup> and only samples with >99.5% concordance were taken forward for subsequent analysis. An ensemble variant calling pipeline (EVC) was used to identify single nucleotide variants (SNV) and short insertions and deletions (indels). EVC implements the SNV and indel variant calling from four variant callers (Mutect2, Strelka2, Varscan2, and MuSE2) and only mutations that are identified by any two variant callers were considered as bona fide mutations<sup>60,62–64</sup>. For N/TERT1 cells, bulk sequencing data from stock were used as a matched normal. For, mouse data, ventral skin from each mouse was used as a matched normal.

**Analysis of mutational signatures.** Analysis of mutational signatures was performed using our previously derived set of reference COSMIC mutational signatures<sup>33</sup> as well as our previously established methodology with the SigProfiler suite of tools used for summarization, simulation, visualization, and assignment of mutational signatures. Mutational matrixes for SBS, DBS and ID were generated with SigProfilerMatrixGenerator (Version 1.2.16)<sup>65,66</sup>. Plotting of each mutational profile was done with sigProfilerPlotting (Version 1.3.13). De novo mutational signature extraction and COSMIC decomposition of de novo signatures were performed with SigProfilerExtractor (Version 1.1.21)<sup>55</sup>. Attribution of COSMIC signatures to each of the samples mutational profile were performed using SigProfilerAssignment (Version 0.0.30)<sup>67</sup>.

**Arsenic co-exposure validation in human cancer.** To evaluate the potential arsenic exposure in human skin cancer through

signature ID13, publicly available whole-genome sequenced skin melanomas and whole-exome sequenced basal cell carcinomas (BCCs) were evaluated. The mutational profiles and mutational signatures in each whole-genome sequenced melanoma were downloaded from a prior publication<sup>22</sup>. Whole-genome sequenced melanomas where both  $\geq 5\%$  of all mutations and  $\geq 100$  mutations were attributed to ID13 were classified as ID13 positive, while all remaining samples were classified as being ID13 negative. For whole-exome sequenced BCCs, somatic mutations were also derived from a prior publication<sup>45</sup>. Mutational signature extractions were performed using SigProfilerExtractor and whole-exome sequenced BCCs with both  $\geq 5\%$  of all mutations and  $\geq 2$  mutations attributed to ID13 were classified as containing the signature.

Normalized mutational profiles and statistical significance testing were performed within R statistical language (Version 4.1.0)<sup>68</sup>. Arrangements of figures and modifications were performed with Adobe Illustrator and BioRender<sup>69</sup>.

**Statistical analysis and reproducibility.** All bar graphs are expressed as the mean  $\pm$  SEM (standard error of the mean) with individual biological replicates shown as corresponding black circles. Since there are multiple distinct groups in the N/TERT1 experiments, one-way ANOVA with Tukey post hoc analysis for multiple comparisons was used to determine significance amongst controls and the samples in the three treatment groups. All cell culture groups have an  $n = 3$  except for the UVR alone group ( $n = 2$ ). Multiplicity adjusted  $p$ -values are reported with significance set to  $p$ -value  $< 0.05$  for all N/TERT1 analyses.

In the mouse study, whole-genome sequencing data were generated for the UVR group using 4 individual animals and for the arsenic plus UVR group using 3 individual animals. FDR-corrected two-sided  $t$ -tests were used to determine significance between UVR and arsenic plus UVR groups in all mouse analyses. FDR-corrections were performed using the Benjamini-Hochberg correction procedure. Significance was determined to be  $q$ -value  $< 0.05$  for all mouse analyses.

In human cancers,  $q$ -values were calculated using FDR-corrected two-sided pairwise  $t$ -tests. FDR-corrections were performed using the Benjamini-Hochberg correction procedure. Statistical significance was set at  $q$ -value  $< 0.05$ . Statistical analysis and plotting were performed using GraphPad Prism v9.3.1.

**Reporting summary.** Further information on research design is available in the Nature Portfolio Reporting Summary linked to this article.

### Data availability

All whole-genome sequencing data have been deposited to Sequence Read Archive (SRA). The sequencing data for N/TERT1 cells can be downloaded using accession number: PRJNA909329 and for SKH-1 mice data with accession number: PRJNA910941. All data and metadata for the previously generated whole-genome sequenced melanoma cancers were obtained from the official PCAWG release (<https://dcc.icgc.org/releases/PCAWG>). Where appropriate, source data are provided for the figures in the paper. The source data for all figures and supplementary figures can be found in Supplementary Data 1. All other data are available from the corresponding authors (or other sources, as applicable) on reasonable request.

### Code availability

Somatic mutations in whole-genome sequencing data were identified using our ensemble variant calling pipeline, which is freely available under the permissive 2-clause BSD license at: <https://github.com/AlexandrovLab/EnsembleVariantCallingPipeline>. All other computational tools utilized in this publication have been mentioned in the methodology section and can be accessed through their respective publications.

Received: 22 February 2023; Accepted: 1 December 2023;

Published online: 16 December 2023

### References

- Barnes, J. L., Zubair, M., John, K., Poirier, M. C. & Martin, F. L. Carcinogens and DNA damage. *Biochem. Soc. Trans.* **46**, 1213–1224 (2018).
- Ames, B. N., Durston, W. E., Yamasaki, E. & Lee, F. D. Carcinogens are mutagens: a simple test system combining liver homogenates for activation and bacteria for detection. *Proc. Natl Acad. Sci.* **70**, 2281–2285 (1973).
- Riva, L. et al. The mutational signature profile of known and suspected human carcinogens in mice. *Nat. Genet.* **52**, 1189–1197 (2020).
- Haverkos, H. W., Haverkos, G. P. & O'Mara, M. Co-carcinogenesis: Human papillomaviruses, coal tar derivatives, and squamous cell cervical cancer. *Front. Microbiol.* **8**, 2253 (2017).
- Rossman, T. G., Uddin, A. N., Burns, F. J. & Bosland, M. C. Arsenite cocarcinogenesis: an animal model derived from genetic toxicology studies. *Environ. Health Perspect.* **110**, 749–752 (2002).
- Kitchin, K. T. Recent advances in arsenic carcinogenesis: modes of action, animal model systems, and methylated arsenic metabolites. *Toxicol. Appl. Pharmacol.* **172**, 249–261 (2001).
- Hughes, M. F., Kenyon, E. M. & Kitchin, K. T. Research approaches to address uncertainties in the risk assessment of arsenic in drinking water. *Toxicol. Appl. Pharmacol.* **222**, 399–404 (2007).
- Hong, Y.-S., Song, K.-H. & Chung, J.-Y. Health effects of chronic arsenic exposure. *J. Prev. Med. Public Health* **47**, 245 (2014).
- Martinez, V. D., Vucic, E. A., Becker-Santos, D. D., Gil, L. & Lam, W. L. Arsenic exposure and the induction of human cancers. *J. Toxicol.* **2011**, 1–13 (2011).
- Mostafa, M. G. & Cherry, N. Arsenic in drinking water, transition cell cancer and chronic cystitis in rural Bangladesh. *Int. J. Environ. Res. Public Health* **12**, 13739–13749 (2015).
- Hartwig, A. et al. Mode of action-based risk assessment of genotoxic carcinogens. *Arch. Toxicol.* **94**, 1787–1877 (2020).
- Zhou, X., Speer, R. M., Volk, L., Hudson, L. G. & Liu, K. J. Arsenic cocarcinogenesis: Inhibition of DNA repair and interaction with zinc finger proteins. in *Seminars in Cancer Biology* Vol. **76**, 86–98 (Academic Press, 2021).
- Chen, Y. et al. Modification of risk of arsenic-induced skin lesions by sunlight exposure, smoking, and occupational exposures in Bangladesh. *Epidemiology* **17**, 459–467 (2006).
- Burns, F. J., Uddin, A. N., Wu, F., Nádas, A. & Rossman, T. G. Arsenic-induced enhancement of ultraviolet radiation carcinogenesis in mouse skin: a dose-response study. *Environ. Health Perspect.* **112**, 599–603 (2004).
- Ding, W., Hudson, L. G., Sun, X., Feng, C. & Liu, K. J. As (III) inhibits ultraviolet radiation-induced cyclobutane pyrimidine dimer repair via generation of nitric oxide in human keratinocytes. *Free Radic. Biol. Med.* **45**, 1065–1072 (2008).
- Rossman, T. G., Uddin, A. N. & Burns, F. J. Evidence that arsenite acts as a cocarcinogen in skin cancer. *Toxicol. Appl. Pharmacol.* **198**, 394–404 (2004).
- Chatterjee, N. & Walker, G. C. Mechanisms of DNA damage, repair, and mutagenesis. *Environ. Mol. Mutagen.* **58**, 235–263 (2017).
- Muenyi, C. S., Ljungman, M. & States, J. C. Arsenic disruption of DNA damage responses—potential role in carcinogenesis and chemotherapy. *Biomolecules* **5**, 2184–2193 (2015).
- Tam, L. M., Price, N. E. & Wang, Y. Molecular mechanisms of arsenic-induced disruption of DNA repair. *Chem. Res. Toxicol.* **33**, 709–726 (2020).
- Alexandrov, L. B. et al. Signatures of mutational processes in human cancer. *Nature* **500**, 415–421 (2013).
- Alexandrov, L. B., Nik-Zainal, S., Wedge, D. C., Campbell, P. J. & Stratton, M. R. Deciphering signatures of mutational processes operative in human cancer. *Cell Rep.* **3**, 246–259 (2013).
- Alexandrov, L. B. et al. The repertoire of mutational signatures in human cancer. *Nature* **578**, 94–101 (2020).
- Martinez, V. D. et al. Whole-genome sequencing analysis identifies a distinctive mutational spectrum in an arsenic-related lung tumor. *J. Thorac. Oncol.* **8**, 1451–1455 (2013).
- Kucab, J. E. et al. A compendium of mutational signatures of environmental agents. *Cell* **177**, 821–836 (2019).
- Hayward, N. K. et al. Whole-genome landscapes of major melanoma subtypes. *Nature* **545**, 175–180 (2017).
- Martincorena, I. et al. High burden and pervasive positive selection of somatic mutations in normal human skin. *Science* **348**, 880–886 (2015).
- Nik-Zainal, S. et al. The genome as a record of environmental exposure. *Mutagenesis* **30**, 763–770 (2015).

28. Rawson, R. V. et al. Unexpected UVR and non-UVR mutation burden in some acral and cutaneous melanomas. *Lab. Invest.* **97**, 130–145 (2017).
29. Saini, N. et al. The impact of environmental and endogenous damage on somatic mutation load in skin fibroblasts. *PLoS Genet.* **12**, e1006385 (2016).
30. Pfeifer, G. P. & Besaratinia, A. UV wavelength-dependent DNA damage and human non-melanoma and melanoma skin cancer. *Photochem. Photobiol. Sci.* **11**, 90–97 (2012).
31. Moreno, N. C. et al. Whole-exome sequencing reveals the impact of UVA light mutagenesis in xeroderma pigmentosum variant human cells. *Nucleic Acids Res.* **48**, 1941–1953 (2020).
32. Jin, S.-G., Padron, F. & Pfeifer, G. P. UVA Radiation, DNA Damage, and Melanoma. *ACS Omega* **7**, 32936–32948 (2022).
33. Tate, J. G. et al. COSMIC: the catalogue of somatic mutations in cancer. *Nucleic Acids Res.* **47**, D941–D947 (2019).
34. Dickson, M. A. et al. Human keratinocytes that express hTERT and also bypass a p16INK4a-enforced mechanism that limits life span become immortal yet retain normal growth and differentiation characteristics. *Mol. Cell. Biol.* **20**, 1436–1447 (2000).
35. Zhivagui, M., Korenjak, M. & Zavadil, J. Modelling mutation spectra of human carcinogens using experimental systems. *Basic Clin. Pharmacol. Toxicol.* **121**, 16–22 (2017).
36. Cooper, K., Yager, J. & Hudson, L. Melanocytes and keratinocytes have distinct and shared responses to ultraviolet radiation and arsenic. *Toxicol. Lett.* **224**, 407–415 (2014).
37. Thompson, B. C., Halliday, G. M. & Damian, D. L. Nicotinamide enhances repair of arsenic and ultraviolet radiation-induced DNA damage in HaCaT keratinocytes and ex vivo human skin. *PLoS One* **10**, e0117491 (2015).
38. Cooper, K. L. et al. Contribution of NADPH oxidase to the retention of UVR-induced DNA damage by arsenic. *Toxicol. Appl. Pharmacol.* **434**, 115799 (2022).
39. Benavides, F., Oberyzy, T. M., VanBuskirk, A. M., Reeve, V. E. & Kusewitt, D. F. The hairless mouse in skin research. *J. Dermatol. Sci.* **53**, 10–18 (2009).
40. Acrylamide, O. National Primary Drinking Water Regulations. *Kidney* **2**, 07 (2009).
41. Ayotte, J. D., Medalie, L., Qi, S. L., Backer, L. C. & Nolan, B. T. Estimating the high-arsenic domestic-well population in the conterminous United States. *Environ. Sci. Technol.* **51**, 12443–12454 (2017).
42. Koller, B. H. et al. Arsenic metabolism in mice carrying a BORCS7/AS3MT locus humanized by syntenic replacement. *Environ. Health Perspect.* **128**, 087003 (2020).
43. Vahter, M. Methylation of inorganic arsenic in different mammalian species and population groups. *Sci. Prog.* **82**, 69–88 (1999).
44. Samanta, G., Sharma, R., Roychowdhury, T. & Chakraborti, D. Arsenic and other elements in hair, nails, and skin-scales of arsenic victims in West Bengal, India. *Sci. Total Environ.* **326**, 33–47 (2004).
45. Bonilla, X. et al. Genomic analysis identifies new drivers and progression pathways in skin basal cell carcinoma. *Nat. Genet.* **48**, 398–406 (2016).
46. Pan-cancer analysis of whole genomes. *Nature* **578**, 82–93 (2020).
47. Ikehata, H. Mechanistic considerations on the wavelength-dependent variations of UVR genotoxicity and mutagenesis in skin: the discrimination of UVA-signature from UV-signature mutation. *Photochem. Photobiol. Sci.* **17**, 1861–1871 (2018).
48. Cooper, K. L., King, B. S., Sandoval, M. M., Liu, K. J. & Hudson, L. G. Reduction of arsenite-enhanced ultraviolet radiation-induced DNA damage by supplemental zinc. *Toxicol. Appl. Pharmacol.* **269**, 81–88 (2013).
49. Huestis, J. et al. Kinetics and thermodynamics of zinc (II) and arsenic (III) binding to XPA and PARP-1 zinc finger peptides. *J. Inorg. Biochem.* **163**, 45–52 (2016).
50. Zhou, X., Cooper, K. L., Sun, X., Liu, K. J. & Hudson, L. G. Selective sensitization of zinc finger protein oxidation by reactive oxygen species through arsenic binding. *J. Biol. Chem.* **290**, 18361–18369 (2015).
51. Zhou, X. et al. Arsenite interacts selectively with zinc finger proteins containing C3H1 or C4 motifs. *J. Biol. Chem.* **286**, 22855–22863 (2011).
52. Nik-Zainal, S. et al. Landscape of somatic mutations in 560 breast cancer whole-genome sequences. *Nature* **534**, 47–54 (2016).
53. Bérubé, R., Desgarnier, M.-C. D., Douki, T., Lechasseur, A. & Rochette, P. J. Persistence and tolerance of DNA damage induced by chronic UVB irradiation of the human genome. *J. Invest. Dermatol.* **138**, 405–412 (2018).
54. Rastogi, R. P., Kumar, A., Tyagi, M. B. & Sinha, R. P. Molecular mechanisms of ultraviolet radiation-induced DNA damage and repair. *J. Nucleic Acids* **2010**, 1–32 (2010).
55. Islam, S. A. et al. Uncovering novel mutational signatures by de novo extraction with SigProfilerExtractor. *Cell Genom.* **2**, 100179 (2022).
56. Smits, J. P. et al. Immortalized N/TERT keratinocytes as an alternative cell source in 3D human epidermal models. *Sci. Rep.* **7**, 1–14 (2017).
57. Wise, J. P. Sr, Wise, S. S. & Little, J. E. The cytotoxicity and genotoxicity of particulate and soluble hexavalent chromium in human lung cells. *Mutat. Res./Genet. Toxicol. Environ. Mutagenesis* **517**, 221–229 (2002).
58. Andrews, S. (Babraham Bioinformatics, Babraham Institute, Cambridge, United Kingdom), (2010).
59. Pedersen, B. S. & Quinlan, A. R. Mosdepth: quick coverage calculation for genomes and exomes. *Bioinformatics* **34**, 867–868 (2018).
60. McKenna, A. et al. The Genome Analysis Toolkit: a MapReduce framework for analyzing next-generation DNA sequencing data. *Genome Res.* **20**, 1297–1303 (2010).
61. Bergmann, E. A., Chen, B.-J., Arora, K., Vacic, V. & Zody, M. C. Conpair: concordance and contamination estimator for matched tumor–normal pairs. *Bioinformatics* **32**, 3196–3198 (2016).
62. Fan, Y. et al. MuSE: accounting for tumor heterogeneity using a sample-specific error model improves sensitivity and specificity in mutation calling from sequencing data. *Genome Biol.* **17**, 1–11 (2016).
63. Kim, S. et al. Strelka2: fast and accurate calling of germline and somatic variants. *Nat. Methods* **15**, 591–594 (2018).
64. Koboldt, D. C. et al. VarScan 2: somatic mutation and copy number alteration discovery in cancer by exome sequencing. *Genome Res.* **22**, 568–576 (2012).
65. Bergstrom, E. N. et al. SigProfilerMatrixGenerator: a tool for visualizing and exploring patterns of small mutational events. *BMC Genom.* **20**, 1–12 (2019).
66. Khandekar, A. et al. Visualizing and exploring patterns of large mutational events with SigProfilerMatrixGenerator. *bioRxiv*. <https://doi.org/10.1101/2023.02.03.527015> (2023).
67. Diaz-Gay, M. et al. Assigning mutational signatures to individual samples and individual somatic mutations with SigProfilerAssignment. *bioRxiv*. <https://doi.org/10.1101/2023.07.10.548264> (2023).
68. Team, R. C. R.: A language and environment for statistical computing. (2013).
69. Perkel, J. M. The software that powers scientific illustration. *Nature* **582**, 137–139 (2020).

## Acknowledgements

Research reported in this publication was supported by the National Institute of Environmental Health Sciences [R01ES030993 to K.J.L./L.G.H.], pilot grant (to L.G.H./K.J.L.) and postdoctoral matching support (to R.M.S.) by University of New Mexico Comprehensive Cancer Center through NIH/NCI grant [P30CA118100], and UNM Center for Metals in Biology and Medicine through NIH/NIGMS grant P20GM130422. Research performed for this publication at the Alexandrov Lab was supported by a Packard Fellowship for Science and Engineering as well as by grants from the US National Institutes of Health, including: NIEHS R01ES030993 (K.J.L./L.G.H.), NIEHS R01ES032547 (L.B.A.), and NCI R01CA269919 (L.B.A.). The content is solely the responsibility of the authors and does not necessarily represent the official views of the National Institutes of Health. The funders were not involved in the study design, data collection, analysis and interpretation of the data, the writing of the article, or the decision to submit the article for publication.

## Author contributions

R.M.S.: conceptualization, data curation, formal analysis, funding acquisition, investigation, methodology, supervision, validation, visualization, writing—original draft, writing—review and editing. S.P.N.: conceptualization, data curation, formal analysis, investigation, methodology, validation, visualization, writing—original draft, writing—review and editing. K.L.C.: conceptualization, data curation, formal analysis, investigation, methodology, validation, visualization, writing—original draft, writing—review and editing. X.Z.: conceptualization, data curation, formal analysis, investigation, methodology, validation, visualization, writing—original draft, writing—review and editing. Y.G.: conceptualization, data curation, formal analysis, investigation, methodology, validation, visualization, writing—original draft, writing—review and editing. H.Y.: conceptualization, data curation, formal analysis, investigation, methodology, validation, visualization, writing—original draft, writing—review and editing. L.G.H.: conceptualization, data curation, formal analysis, funding acquisition, investigation, methodology, project administration, resources, software, supervision, validation, visualization, writing—review and editing. L.B.A.: conceptualization, data curation, formal analysis, funding acquisition, investigation, methodology, project administration, resources, software, supervision, validation, visualization, writing—review and editing. K.J.L.: conceptualization, data curation, formal analysis, funding acquisition, investigation, methodology, project administration, resources, software, supervision, validation, visualization, writing—review and editing.

## Competing interests

L.B.A. is a co-founder, CSO, scientific advisory member, and consultant for io9, has equity and receives income. The terms of this arrangement have been reviewed and approved by the University of California, San Diego in accordance with its conflict of interest policies. L.B.A.'s spouse is an employee of Biotheranostics. L.B.A. declares U.S. provisional applications with serial numbers: 63/289,601; 63/269,033; 63/483,237; 63/366,392. L.B.A. and S.P.N. also declare U.S. provisional applications with serial numbers: 63/412,835 and 63/492,348. All other authors declare they have no known competing interests or personal relationships that could have appeared to influence the work reported in this paper.

**Additional information**

**Supplementary information** The online version contains supplementary material available at <https://doi.org/10.1038/s42003-023-05659-4>.

**Correspondence** and requests for materials should be addressed to Ludmil B. Alexandrov or Ke Jian Liu.

**Peer review information** *Communications Biology* thanks Erik Larsson, Javier Herrero, and the other, anonymous, reviewer(s) for their contribution to the peer review of this work. Primary Handling Editor: David Favero.

**Reprints and permission information** is available at <http://www.nature.com/reprints>

**Publisher's note** Springer Nature remains neutral with regard to jurisdictional claims in published maps and institutional affiliations.



**Open Access** This article is licensed under a Creative Commons Attribution 4.0 International License, which permits use, sharing, adaptation, distribution and reproduction in any medium or format, as long as you give appropriate credit to the original author(s) and the source, provide a link to the Creative Commons licence, and indicate if changes were made. The images or other third party material in this article are included in the article's Creative Commons licence, unless indicated otherwise in a credit line to the material. If material is not included in the article's Creative Commons licence and your intended use is not permitted by statutory regulation or exceeds the permitted use, you will need to obtain permission directly from the copyright holder. To view a copy of this licence, visit <http://creativecommons.org/licenses/by/4.0/>.

© The Author(s) 2023